Initial preclinical evaluation of 18F-fluorodeoxysorbitol PET as a novel functional renal imaging agent

H. Wakabayashi, R. A. Werner, N. Hayakawa, M. S. Javadi, C. Xinyu, K. Herrmann, S. P. Rowe, Constantin Lapa, T. Higuchi

Angaben zur Veröffentlichung / Publication details:

Wakabayashi, H., R. A. Werner, N. Hayakawa, M. S. Javadi, C. Xinyu, K. Herrmann, S. P. Rowe, Constantin Lapa, and T. Higuchi. 2016. "Initial preclinical evaluation of 18F-fluorodeoxysorbitol PET as a novel functional renal imaging agent." *Journal of Nuclear Medicine* 57 (10): 1625–28. https://doi.org/10.2967/jnumed.116.172718.

Initial Preclinical Evaluation of ^{18}F-Fluorodeoxysorbitol PET as a Novel Functional Renal Imaging Agent

Hiroshi Wakabayashi*[1], Rudolf A. Werner*[1,2], Nobuyuki Hayakawa[1], Mehrbod S. Javadi[3], Chen Xinyu[1,2], Ken Herrmann[1], Steven P. Rowe[3], Constantin Lapa†[1], and Takahiro Higuchi†[1,2]

[1]Department of Nuclear Medicine, University of Würzburg, Würzburg, Germany; [2]Comprehensive Heart Failure Center, University of Würzburg, Würzburg, Germany; and [3]Division of Nuclear Medicine and Molecular Imaging, The Russell H. Morgan Department of Radiology and Radiological Science, Johns Hopkins University, Baltimore, Maryland

The kidneys are responsible for various important functions within the body including waste excretion, fluid regulation, acid-base homeostasis, and hormone secretion. Glomerular filtration rate (GFR) is considered the best indicator of overall kidney function for early monitoring and optimization of therapeutic interventions (*1,2*). However, the accurate quantification of GFR, which is of particular importance in the setting of clinical research, still remains challenging (*3,4*). Measurement of exogenous inulin or radiolabeled markers such as ^{51}Cr-labeled ethylenediaminetetraacetic acid (EDTA) urinary clearance is considered the gold standard, but the application is limited because strict adherence to multiple time points of urine collection involving catheterization is required. Serum creatinine concentration is the most commonly used surrogate marker for GFR and depends on endogenous creatinine production, which differs in association with changes in diet and total-body muscle mass.

Dynamic planar renography using ^{99m}Tc-DTPA is an established tool for noninvasive evaluation of renal pathophysiology in clinical practice (*5–7*). However, because of the limited temporal and spatial resolution of the detection systems, local assessment of tracer distribution in tomographic images is not feasible. Furthermore, absolute quantification of ^{99m}Tc-DTPA is sometimes limited because established compensation algorithms for tissue attenuation and scatter are suboptimal with 2-dimensional planar imaging. In contrast, the intrinsic advantages of PET could potentially offer superior spatial and temporal resolutions. These coincidence detection-based advantages enable accurate quantification in 3-dimensional tomography. However, as of yet, the use of clinical renal PET has been limited because of the lack of appropriate available and affordable PET tracers (*8*).

2-deoxy-2-^{18}F-fluorodeoxysorbitol (^{18}F-FDS), an analog of sorbitol, can be easily synthesized via a 1-step reduction of ^{18}F-FDG, which is readily available (*9–11*). In early human studies, sorbitol urinary clearance was reported to be identical to inulin clearance (sorbitol–to–inulin clearance ratio = 1.01) (*12*). Therefore, we hypothesized that radiolabeled ^{18}F-FDS is also filtered at the renal glomerulus and thereby can be used for GFR measurements by PET imaging. In these presented initial animal experiments, we

For correspondence contact: Takahiro Higuchi, Department of Nuclear Medicine/Comprehensive Heart Failure Center, University of Würzburg, Oberdürrbacher Strasse 6, 97080 Würzburg, Germany
E-mail: thiguchi@ukw.de
*Contributed equally to this work.
†Contributed equally to this work.

determined the basic biodistribution properties of ^{18}F-FDS as a renal PET compound including clearance through the renal-collecting system pathway, plasma protein binding, and metabolic transformation.

MATERIALS AND METHODS

Animals

Healthy male Wistar rats weighing 200–250 g were used ($n = 25$). Experimental protocols were approved by the regional governmental commission of animal protection and conducted in strict performance according to the *Guide for the Care and Use of Laboratory Animals* (*13*).

Tracer Production

^{18}F-FDS was synthesized following a previously described procedure (*9*). In short, $NaBH_4$ (2 mg, 0.053 mmol) was added to a solution of ^{18}F-FDG in saline, and the resulting mixture was stirred at 35°C for 15 min. After the reaction was quenched, the mixture was adjusted to a pH of 7.4 and filtered through an Alumina-N Sep-Pak cartridge (Waters). The filtrate was then reconstituted in saline and passed through a 0.22-μm Millipore filter into a sterile multidose vial for in vitro and in vivo experiments. The radiochemical purity of the ^{18}F-FDS was confirmed by radio–thin-layer chromatography (CR 35 BIO; Dürr Medical) (80% acetonitrile with 20% water as eluent). Analysis at the end of syntheses revealed a radiochemical purity greater than 95% of the radiolabeled compound.

DTPA kits (Fujifilm RI Pharma) were labeled using generator-produced ^{99m}Tc-pertechnetate according to the provided procedure.

PET Imaging

Five rats were studied with a high-resolution (1.2- to 1.5-mm spatial resolutions at the center of the field of view) dedicated small-animal PET system (Inveon microPET; Siemens). Animals were maintained under anesthesia by 2% isoflurane during the whole experiment. ^{18}F-FDS (30 MBq) was administered via the tail vein. A 35-min list-mode PET acquisition was started shortly before tracer injection. The data were sorted into 3-dimensional sonograms, which were then rebinned with a Fourier algorithm to reconstruct dynamic images using a 2-dimensional ordered-subset expectation maximization method. The reconstructed dynamic images consisted of the 61 frames acquired (15 frames × 8 s, 26 frames × 30 s, and 20 frames × 60 s). All reconstructed images were corrected for ^{18}F decay, random coincidences, and dead time; correction for attenuation was not performed.

The obtained PET images were analyzed with the public domain AMIDE imaging software (version 1.01). Regions of interest were manually placed for cortical regions excluding the medulla and collecting systems on 5 consecutive middle coronal sections of the kidneys as described elsewhere (*14*). The mean radioactivity concentration within the region of interest in each frame was measured as percentage injected dose per centimeter cubed. Then, time–activity curves (renography) were generated, and the time of maximal and half maximal concentration were calculated.

Postmortem Tissue Counting

Rats were simultaneously injected with ^{18}F-FDS (10 MBq) and ^{99m}Tc-DTPA (1.5 MBq) through a tail vein catheter under anesthesia with 2% isoflurane. The rats were euthanized at 10 ($n = 5$), 30 ($n = 4$), and 60 min ($n = 5$) after tracer administration. Then, organs of interest (blood, liver, intestine, muscle, spleen, stomach, bone, heart, and lung) were collected, weighed, and counted for radioactivity in an automated γ-counter (Wizard; PerkinElmer). Tissue radioactivity concentrations were estimated and expressed as injected dose per gram (%ID/g) of each organ sample.

In Vivo Stability and Plasma Protein Binding

Samples of blood were obtained via the tail vein at 10 ($n = 2$) and 35 min ($n = 4$) after intravenous administration of ^{18}F-FDS (30 MBq). To obtain the plasma fractions, the collected blood samples were immediately centrifuged. The rats were euthanized at 35 min after tracer administration. Then, urine samples in the bladder were carefully collected by laparotomy. The stability of ^{18}F-FDS was determined by radiolabeled thin-layer chromatography (Silica gel $60F_{254}$; Merck KGaA) in the methanol-extracted plasma and urine samples. Binding of ^{18}F-FDS to plasma proteins was determined using a centrifugal filter device (Centrifree; Merck Millipore) and calculated as (1 − [filtered plasma counts/plasma counts]) × 100.

Statistics

Data are presented as mean ± SD. Comparisons between ^{18}F-FDS and ^{99m}Tc-DTPA values were made with the Student t test for independent samples. A P value of less than 0.05 was considered statistically significant. Statistical analysis was performed using the software package JMP (SAS Institute).

RESULTS

Systemic ^{18}F-FDS Distribution

Dynamic whole-body PET imaging revealed high renal tracer excretion with low hepatobiliary clearance (Fig. 1A). Intense and rapid tracer accumulation in the kidneys and time-dependent increase of tracer uptake in the bladder were observed without any obvious signals from other organs.

In vivo biodistribution was evaluated at 10, 30, and 60 min after ^{18}F-FDS administration. The kidneys exhibited the highest tracer concentration among all organs and remained highest at all time points. Tracer concentration in the liver was almost as high as blood levels at all time points. Furthermore, the radioactive concentration in the intestine remained unchanged, suggesting considerably low hepatobiliary clearance and exclusive kidney secretion of ^{18}F-FDS. Tracer uptake in the muscle, spleen, stomach, bone, heart, and lung remained low. The results of the postmortem tissue-counting study are summarized in Table 1.

Biodistribution of ^{18}F-FDS and ^{99m}Tc-DTPA was directly compared in the same animals by ex vivo tissue analysis after dual tracer administration (Table 1). Both tracers showed a highly comparable biodistribution pattern, with high kidney clearance and low activity in other organs at all time points. ^{99m}Tc-DTPA concentrations in the blood and liver were slightly lower than those of ^{18}F-FDS.

PET Renography

Examples of PET renography after ^{18}F-FDS administration and a PET-derived renography curve are shown in Figures 1B and 1C. After strong visualization of the inferior vena cava immediately after tracer administration via the tail vein (0–8 s), tracer uptake in the renal cortex was observed at the second frame (8–16 s). Transient increase of the cortical tracer uptake and transition of the activity into the collecting system were nicely depicted in tomographic views. Split renography curves were generated to estimate functional parameters: the time of maximal concentration was measured to be 2.8 ± 1.2 and 2.9 ± 1.5 min, and the time of half maximal concentration was found to be 8.8 ± 3.7 and 11.1 ± 4.9 min, for right and left kidneys, respectively.

In Vivo Stability and Plasma Protein Binding

Radio–thin-layer chromatography analysis of plasma and urine samples and ^{18}F-FDS solution revealed completely matched

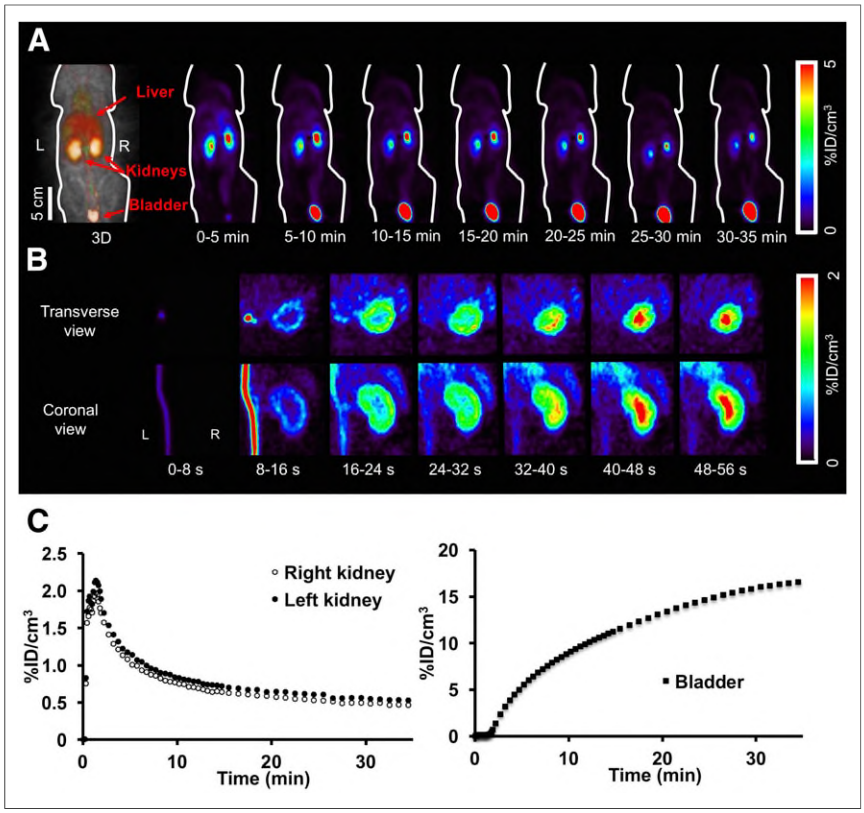

FIGURE 1. Results of in vivo ^{18}F-FDS PET imaging. (A) Whole-body dynamic PET images in coronal view. High tracer secretion exclusively via kidneys and time-dependent increase of bladder activity are seen. (B) Dynamic right kidney images of transverse and coronal views. Rapid tracer accumulation in renal cortex and tracer transit into collecting system can be observed. (C) Examples of time–activity curves of kidneys (left) and bladder (right) assessed by dynamic PET imaging. %ID/cm^3 = percentage injected dose per centimeter cubed.

single spots in all samples, indicating the nonexistence of radiolabeled metabolites in blood and urine at 35 min after tracer administration.

In vivo serum protein binding of ^{18}F-FDS at 10 and 35 min after tracer administration was quantified as minimal (less than 0.1%) by separation of free ^{18}F-FDS using ultrafiltration.

DISCUSSION

The present small-animal study demonstrates the potential feasibility of ^{18}F-FDS as a novel PET tracer for functional renal imaging.

High renal excretion of ^{18}F-FDS in the same manner as the reference conventional tracer ^{99m}Tc-DTPA was confirmed with in vivo tissue-counting and imaging experiments. ^{99m}Tc-DTPA is known to be solely excreted rapidly via the glomerulus without tubular reabsorption or secretion and thereby widely used for functional imaging and GFR estimation. The results of our study suggest that ^{18}F-FDS might also be freely filtered at the renal glomerulus. This is consistent with results of earlier studies that determined renal excretion of several hexitols including sorbitol (*12*). Rapid clearance of exogenous sorbitol completely identical with inulin clearance measured in dogs and humans could be demonstrated by exclusive glomerular filtration and absence of tubular excretion and reabsorption, as would be suggested by the results in these studies.

Plasma protein binding significantly influences radionuclide tracer kinetics and is one of the key characteristics for GFR estimation. Only the free fraction of the tracer is filtered at the glomerulus, whereas the fraction of tracer binding to the protein remains in the blood,

TABLE 1
Postmortem Tissue Counting in Rats at 10 Minutes, 30 Minutes, and 1 Hour After Injection of ^{18}F-FDS and ^{99m}Tc-DTPA

Organ	^{18}F-FDS			^{99m}Tc-DTPA		
	10 min	30 min	1 h	10 min	30 min	1 h
Blood	0.61 ± 0.16	0.38 ± 0.03*	0.15 ± 0.01*	0.84 ± 0.18	0.34 ± 0.03	0.09 ± 0.02
Liver	0.54 ± 0.10*	0.31 ± 0.03*	0.11 ± 0.01†	0.34 ± 0.09	0.15 ± 0.01	0.05 ± 0.01
Kidneys	1.77 ± 0.74	1.21 ± 0.09*	0.53 ± 0.21	2.51 ± 0.97	1.50 ± 0.18	0.77 ± 0.27
Intestine	0.17 ± 0.05	0.15 ± 0.02*	0.10 ± 0.01†	0.14 ± 0.03	0.08 ± 0.03	0.04 ± 0.01
Muscle	0.14 ± 0.04*	0.13 ± 0.03	0.05 ± 0.01*	0.20 ± 0.04	0.16 ± 0.04	0.02 ± 0.01
Spleen	0.18 ± 0.05	0.22 ± 0.01†	0.12 ± 0.01	0.16 ± 0.03	0.11 ± 0.01	0.10 ± 0.17
Stomach	0.08 ± 0.02	0.12 ± 0.06	0.03 ± 0.01	0.11 ± 0.03	0.12 ± 0.06	0.02 ± 0.01
Bone	0.14 ± 0.04	0.08 ± 0.01	0.05 ± 0.01†	0.15 ± 0.04	0.07 ± 0.02	0.02 ± 0.01
Heart	0.26 ± 0.07	0.21 ± 0.01*	0.13 ± 0.01*	0.30 ± 0.07	0.14 ± 0.01	0.05 ± 0.03
Lung	0.47 ± 0.16	0.34 ± 0.06	0.17 ± 0.02*	0.63 ± 0.24	0.31 ± 0.07	0.09 ± 0.06

*$P < 0.05$ vs. ^{99m}Tc-DTPA.
†$P < 0.0001$ vs. ^{99m}Tc-DTPA.
Data are %ID/g (mean value ± SD). Number of rats was 5 at 10 min, 4 at 30 min, and 5 at 1 h after tracer injection.

potentially causing significant underestimation of glomerular filtration. Protein binding of ^{99m}Tc-DTPA has been reported to be around 2%–10% (*5,15*). Our results demonstrate ^{18}F-FDS plasma protein binding rates less than 0.1%. These are considerably lower and suggest ^{18}F-FDS as a preferred agent for GFR estimation.

Tracer metabolism affects quantitative parameters in PET imaging. The high stability of ^{18}F-FDS was confirmed in this study, and no metabolites were detected in the samples of urine and blood at 35 min after tracer administration. Consistently, tracer accumulation in the bone was not observed, suggesting the absence of free ^{18}F-fluoride as a result of tracer degradation.

PET imaging has many advantages over conventional planar renography. PET allows accurate tracer detection using established compensation algorithms for soft-tissue body attenuation and provides higher spatial and temporal resolution. These properties enable dynamic imaging with 3-dimensional tomography for more accurate and quantifiable datasets. Regional tracer concentrations at multiple time points are provided in absolute values of tracer concentrations. Therefore, several PET tracers have been developed as potential candidates for quantitative renal imaging including ^{68}Ga- and ^{18}F-labeled compounds (*16–18*). One of the most promising tracers is ^{68}Ga-EDTA, which was recently introduced for renal PET imaging (*19,20*). In a clinical study comprising 31 patients, Hofman et al. (*20*) confirmed good agreement of GFR estimation with ^{68}Ga-EDTA PET and ^{51}Cr-EDTA plasma clearance. A disadvantage of ^{68}Ga-labeled tracers is the requirement of costly on-site generators, although the availability of ^{68}Ga is currently improving because of the increased use for somatostatin receptor PET imaging. In contrast, ^{18}F-labeled imaging agents have a longer half-life (110 min), allowing for cost reduction by delivering from central cyclotron production sites. Additionally, in comparison with other positron-emitting radionuclides (such as ^{68}Ga), the shorter positron range offers better image quality with higher temporal resolution. ^{18}F-FDS has the additional advantage of easy synthesis involving a simple 1-step reduction of ^{18}F-FDG. Because ^{18}F-FDG is the most commonly used clinical PET tracer, virtually any PET facility worldwide would have access to this tracer. The potential of broad clinical application replacing conventional renal scintigraphy can be speculated on, although confirmatory studies including cost-effectiveness analyses are needed to determine the appropriate applications for the renal PET imaging.

CONCLUSION

^{18}F-FDS demonstrated promising properties for renal PET imaging, with high renal excretion, low serum protein binding, and high in vivo stability in rat experiments. Advantages include simple ^{18}F-FDS production via reduction of ^{18}F-FDG and the ability to perform dynamic PET acquisitions. Improvements in functional renal imaging over conventional techniques may have important clinical impact. Further validation in large animal models and early human clinical trials is warranted.

DISCLOSURE

The costs of publication of this article were defrayed in part by the payment of page charges. Therefore, and solely to indicate this fact, this article is hereby marked "advertisement" in accordance with 18 USC section 1734. This work was supported by the Competence Network of Heart Failure funded by the Integrated Research and Treatment Center of the Federal Ministry of Education and Research and German Research Council (HI 1789/2-1). Hiroshi Wakabayashi received a postdoctoral research fellowship from The Uehara Memorial Foundation for the research in overseas. No other potential conflict of interest relevant to this article was reported.

REFERENCES

1. Herrler T, Wang H, Tischer A, et al. Decompression of inflammatory edema along with endothelial cell therapy expedites regeneration after renal ischemia-reperfusion injury. *Cell Transplant.* 2013;22:2091–2103.
2. Herrler T, Wang H, Tischer A, et al. ^{99m}Tc-MAG3 scintigraphy for the longitudinal follow-up of kidney function in a mouse model of renal ischemia-reperfusion injury. *EJNMMI Res.* 2012;2:2.
3. Killion D, Nitzsche E, Choi Y, Schelbert H, Rosenthal JT. Positron emission tomography: a new method for determination of renal function. *J Urol.* 1993;150:1064–1068.
4. Werner RA, Bluemel C, Lapa C, et al. Pretherapeutic estimation of kidney function in patients treated with peptide receptor radionuclide therapy: can renal scintigraphy be safely omitted? *Nucl Med Commun.* 2014;35:1143–1149.
5. Klopper JF, Hauser W, Atkins HL, Eckelman WC, Richards P. Evaluation of ^{99m}Tc-DTPA for the measurement of glomerular filtration rate. *J Nucl Med.* 1972;13:107–110.
6. Hilson AJ. Functional renal imaging with nuclear medicine. *Abdom Imaging.* 2003;28:176–179.
7. Taylor AT. Radionuclides in nephrourology, part 1: radiopharmaceuticals, quality control, and quantitative indices. *J Nucl Med.* 2014;55:608–615.
8. Szabo Z, Xia J, Mathews WB, Brown PR. Future direction of renal positron emission tomography. *Semin Nucl Med.* 2006;36:36–50.
9. Li ZB, Wu Z, Cao Q, et al. The synthesis of ^{18}F-FDS and its potential application in molecular imaging. *Mol Imaging Biol.* 2008;10:92–98.
10. Weinstein EA, Ordonez AA, DeMarco VP, et al. Imaging enterobacteriaceae infection in vivo with F-18-fluorodeoxysorbitol positron emission tomography. *Sci Transl Med.* 2014;6:259ra146.
11. Bar-Shalom R, Yefremov N, Guralnik L, et al. Clinical performance of PET/CT in evaluation of cancer: additional value for diagnostic imaging and patient management. *J Nucl Med.* 2003;44:1200–1209.
12. Willie W, Smith NF, Homer W. Smith. Renal excretion of hexitols (sorbitol, mannitol, and dulcitol) and their derivatives (sorbitan, isomannide, and sorbide) and of endogenous creatinine-like chromogen in dog and man. *J Biol Chem.* 1940;135:231–250.
13. *Guide for the Care and Use of Laboratory Animals.* Bethesda, MD: National Institutes of Health; 1985. NIH publication 85-23.
14. Juárez-Orozco LE, Szymanski MK, Hillege HL, et al. Imaging of cardiac and renal perfusion in a rat model with ^{13}N-NH 3 micro-PET. *Int J Cardiovasc Imaging.* 2015;31:213–219.
15. Rehling M. Stability, protein binding and clearance studies of [^{99m}Tc]DTPA: evaluation of a commercially available dry-kit. *Scand J Clin Lab Invest.* 1988;48:603–609.
16. Pathuri G, Sahoo K, Awasthi V, Gali H. Renogram comparison of p-[^{18}F]fluorohippurate with o-[^{125}I]iodohippurate and [^{99}Tc]MAG3 in normal rats. *Nucl Med Commun.* 2011;32:908–912.
17. Lee JY, Jeong JM, Kim YJ, et al. Preparation of Ga-68-NOTA as a renal PET agent and feasibility tests in mice. *Nucl Med Biol.* 2014;41:210–215.
18. Pathuri G, Hedrick AF, January SE, et al. Synthesis and in vivo evaluation of gallium-68-labeled glycine and hippurate conjugates for positron emission tomography renography. *J Labelled Comp Radiopharm.* 2015;58:14–19.
19. Yamashita M, Inaba T, Kawase Y, et al. Quantitative measurement of renal function using Ga-68-EDTA. *Tohoku J Exp Med.* 1988;155:207–208.
20. Hofman M, Binns D, Johnston V, et al. ^{68}Ga-EDTA PET/CT imaging and plasma clearance for glomerular filtration rate quantification: comparison to conventional 51Cr-EDTA. *J Nucl Med.* 2015;56:405–409.